Synergy Between Supported Metal Single Atoms and Nanoparticles and their Relevance in Catalysis

Philippe Serp

ChemCatChem

Review
doi.org/10.1002/cctc.202300545

Chemistry Europe
European Chemical Societies Publishing

www.chemcatchem.org

Synergy Between Supported Metal Single Atoms and Nanoparticles and their Relevance in Catalysis

Philippe Serp*[a]

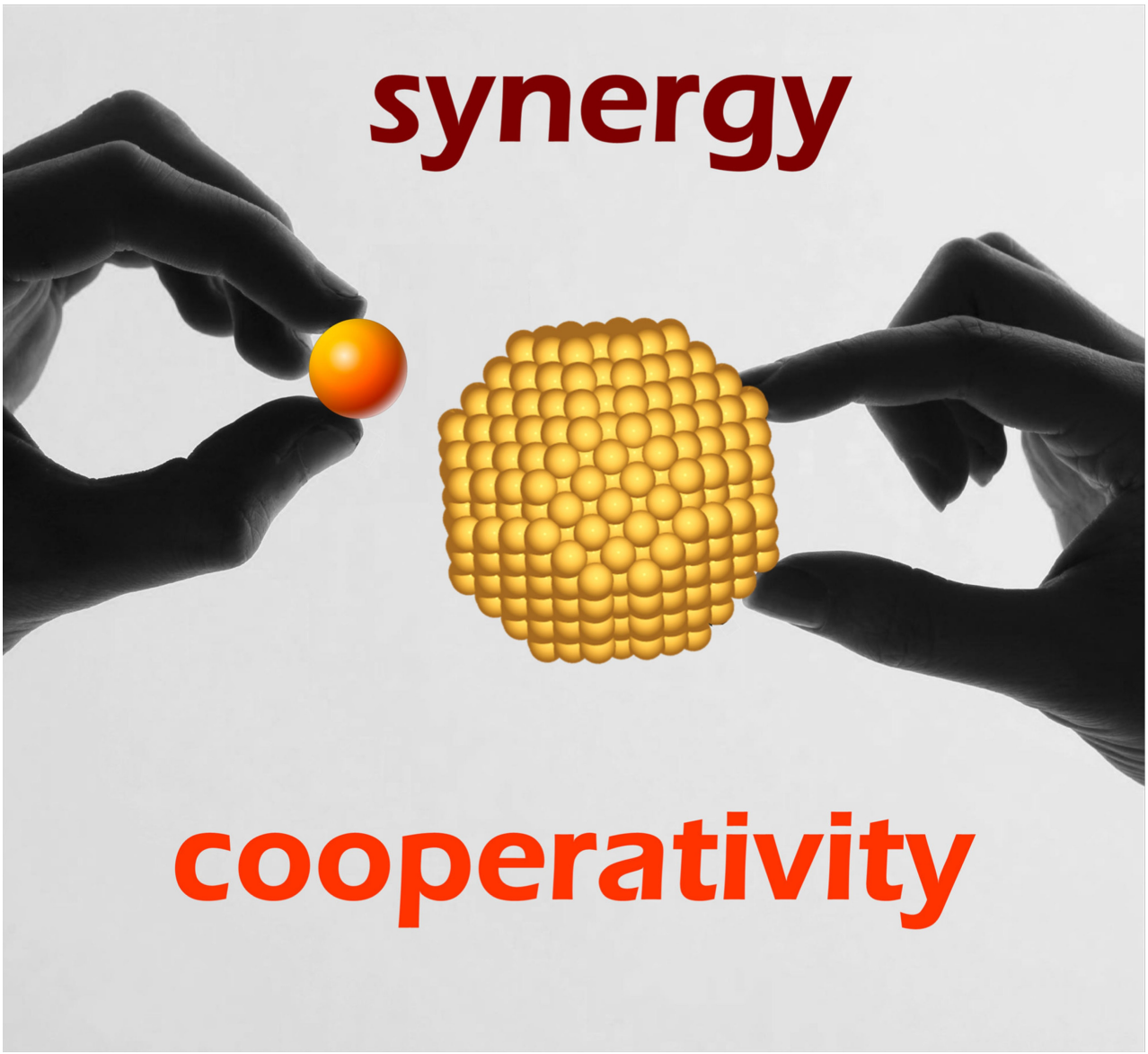

Catalytic active sites consisting in isolated metal single atoms can be found in enzymatic, homogenous and heterogeneous catalysts. In heterogeneous catalysis, single-atom catalysts (SACs) may offer high reactivity and selectivity towards some reactions provided their local coordination environment and electronic properties are correctly tuned. These sites generally possess specific properties compared to metal nanoparticles or clusters. Because of the difficulty, inherent in supported catalysis, of preparing catalysts having a high homogeneity of active sites, these two species have had to coexist in many supported catalysts. If the current trend is often limited to comparing the reactivity of these two types of species, we will see in this mini-review that for few years, work has highlighted a possible synergy between these species to improve catalytic performance. The different types of synergies are discussed, as well as challenges and opportunities for such catalysts in thermal-, electro- and photo-catalysis.

1. Introduction

The use of catalytic entities having only one metal atom is the normality in homogeneous catalysis; and has become since the beginning of this century a prominent research field in supported catalysis.[1] In homogeneous catalysis, the first coordination sphere around the metal ensures the catalytic performance and the stability of the coordination complex, which can if adequately tuned withstand drastic conditions, such as for the Rh- or Ir-catalyzed carbonylation of methanol.[2] The same thing prevails when isolated metal atoms (without molecular ligand) are immobilized on a solid support,[3] and intrinsic thermodynamic stability (chelate effect of the support), kinetic stability and dynamic stability are key factors in determining the reactivity of single atom catalysts (SACs).[4] This extreme limit of the size of the active site (single atom, SA) should be compared to clusters/nanoparticles (NPs) or bulk metal. In homogeneous catalyst systems, there is the persistent problem that metal clustering and aggregation/precipitation cause catalyst decomposition and loss of activity. Pd black formation in reactions of organic synthesis is a typical example.[5] Alternatively, the interconversion of various metal species during catalytic reactions, including molecular complexes, clusters and NPs,[6] have governed the development of the concept of "cocktail catalysis" in some dynamic systems.[7] The transition that operates *via* subnanometric species (clusters), whether in homogeneous or heterogeneous catalysis, induces problems related to the stability of these species and to the control of their activity/selectivity. Indeed, minor changes in their environment, size and composition – such as the addition or removal of a single metal atom – can have a substantial influence on their performances.[8] Consequently, the use of nanoscale metal particles or SAs can lead to more stable systems, both in molecular- and in supported-catalysis, which are generally preferred for industrial applications. Worth to be noted is the dynamic formation of active metal SAs, which can be stabilized on some defects of the support, from metallic NPs acting as ad-atom reservoir,[9] during catalytic reaction. Such phenomenon has been particularly observed in the case of gold catalysts supported on reducible oxide or carbon supports for CO oxidation[10] and acetylene hydrochlorination.[11] In all these examples, the isolated atoms are more active than the NPs for the studied reactions.

In term of reactivity, metal SAs and NPs often present marked differences due to the coverage and ensemble (ensemble of metal atoms in NPs)[12] effects, not present as such for isolated metal species.[13] Works by Sachtler and coworkers in the 90's on the reaction of H/D exchange of cyclopentane on Pt/mordenites were already going in this direction.[14] While these differences in reactivity are often put forward to rationalize catalysis results,[15] it is rarer that they are used to improve the performance of a catalytic system for a given chemical transformation. However, synergistic interaction between SA species and metal NPs have the ability of catalyzing reactions that cannot be easily catalyzed by SAs or metal NPs catalysts. There are still few studies integrating molecular or enzymatic catalytic species together with supported metal NPs;[16] and these studies are limited to cascade reactions. With regard to single atom catalysis, the difficulty of selectively preparing SACs with consequent metal loading means that SAs and NPs may coexist in the catalysts prepared, including industrially.[17] In fact, a growing number of articles have appeared in recent years promoting cooperative catalysis between SAs and NPs present on the same support,[18] and structure-activity relationships are under discussion in literature. Although the approach is interesting, very few studies are still dealing with the use of physical mixtures of catalysts (one containing SAs and the other NPs).[19]

When considering the possible synergy between SAs and NPs on the same support, the question of communication between these two species should be taken into account. Some type of synergy does not involved communication, such as synergy in parallel for cascade reactions (Figure 1a). In that case, either the different active sites exhibit enhanced effects in a catalytic reaction, or they catalyze different reactions separately, resulting in bifunctional effects. For other types of synergy, a communication through the support is operative. This is the case for *d*-band regulation by electron transfer that can improve the catalytic performance by regulating the adsorption strength of the reactants and intermediates, and can contribute to catalyst stabilization (Figure 1b). In that case, features such as metal loading, species proximity and nature of the support

[a] *Prof. Dr. P. Serp*
LCC–CNRS UPR 8241, composante ENSIACET
Université de Toulouse
4 allée Emile Monso
31030 Toulouse (France)
E-mail: philippe.serp@ensiacet.fr

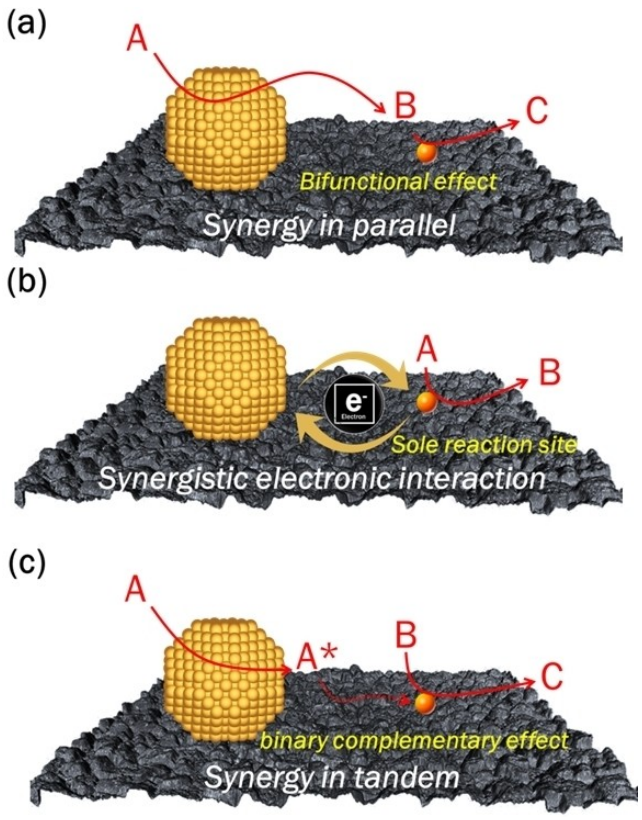

Figure 1. Overview of themes discussed in this article related to synergy between supported metal single atoms and nanoparticles.

should be taken into consideration to exploit cooperativity. Communication is also needed when synergy operates in tandem, which means that SAs and NPs are involved at different steps of a given chemical reaction, like in some hydrogenation reactions where metal NPs activated H_2 and SAs performed the hydrogenation of the substrate (Figure 1c). Different interdisciplinary strategies including experimental and theoretical approaches are required for a holistic understanding of this type of catalysis, which occurs perhaps unknowingly (due to the difficulties of detecting isolated atoms) in many catalytic systems. This mini-review article focuses on present concepts and accompanying future challenges in the field of the possible synergy between supported metal SAs and NPs, highlighting recent developments in catalysis.

Biographical Sketch. Philippe Serp is a Professor of Inorganic Chemistry in Toulouse University. He received his Ph.D. degree from Toulouse University in 1994 and engaged in postdoctoral research at the University of Porto and Louvain-la-Neuve from 1995 to 1997. His research interests in the Laboratory of Coordination Chemistry include the preparation of nanostructured catalytic materials, and molecular approaches to understand supported catalysis; fields in which with coworkers he has published over 200 publications among them twenty European and U.S. patents. His research has been recognized by the Catalysis (2004) and Industrial Chemistry (2012) Division Awards of the French Chemical Society.

2. Synergy in Parallel or Bifunctional Effect

For multistep tandem/cascade catalytic reactions, optimal performances require the engagement of spatially defined multiple distinct catalytic sites with different catalytic properties. Structural heterogeneity as the one obtained in mixtures of SAs and NPs can be beneficial by promoting different individual steps in certain complex multistep reactions.

Biobased 2-substituted benzimidazoles have been prepared *via* a single-step cascade reaction involving dehydrogenation of bio-alcohols and reduction of nitro groups on Co_{SA+NP}/N–C catalysts (N,C=nitrogen-doped carbon support) containing ZnO basic sites (Figure 2a).[20] Catalytic transfer hydrogenative cyclization of 2-nitroaniline and bio-based furfuryl alcohol (FA) toward 2-(2-furyl)1H-benzimidazole was first performed to evaluate the catalyst performance. Experimental results and DFT calculations suggested that Co_{SA} have a higher activity for the dehydrogenation of FA, while Co_{NP} can promote the reduction of 2-nitroaniline. The proposed mechanism involved several steps. First, FA undergoes dehydrogenation on Co_{SA} sites to generate furfural, and 2-nitroaniline borrows the hydrogen

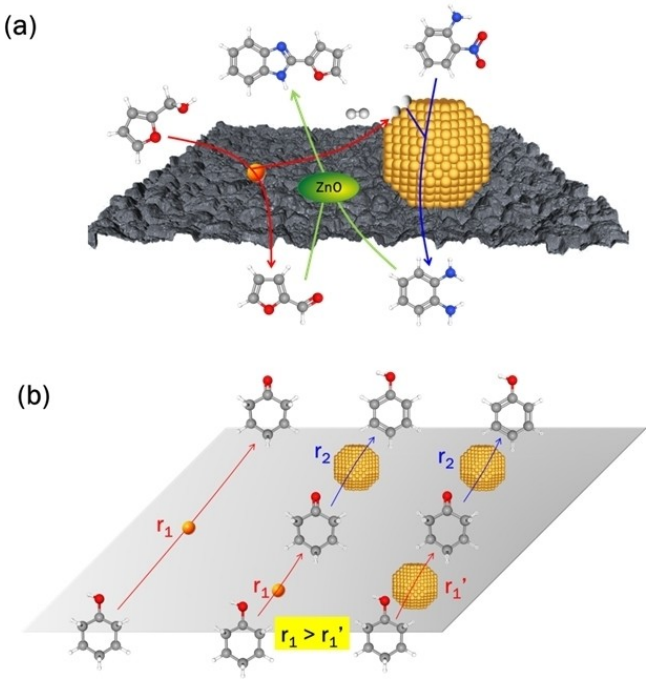

Figure 2. Bifunctional effect for synergy in parallel with supported metal SAs and NPs. (**a**) Reaction routes to bio-based benzimidazoles on Co_{SA-+NP}/N–C catalysts.[18] (**b**) Evaluation of the individual reaction steps of cyclohexanol dehydrogenation over Rh_{SA+NP}/C catalysts and the illustration of proposed reaction pathways.[19]

from FA, followed by reduction to *o*-phenylenediamine under the action of Co_{NP} and Co_{SA}. Then, the two intermediate products, o-phenylenediamine and furfural, undergo C–N coupling cyclization to rapidly generate 2-substituted benzimidazole on ZnO sites (alkaline local environment).

Cyclohexanol dehydrogenation requires a monofunctional behavior (dehydrogenation) but contains two consecutive chemical transformations (cyclohexanol-to-cyclohexanone – R_1, and cyclohexanone-to phenol – R_2) including several C–H and O–H bonds activation.[21] On Rh_{SA+NP}/C catalysts, the Rh_{SA} show the highest activity for R_1, whereas the Rh_{NP} are mainly responsible for R_2 (Figure 2b). The coexistence of Rh_{SA} and Rh_{NP} significantly boosts the overall reaction. Considering the fact that the TOF_{R1}/TOF_{R2} ratio is equal to 6.5, an optimization of the density of the two active sites but above all of their relative proportion (Rh_{SA}/Rh_{NP} ratio) should allow to further enhance the catalyst performance. An efficient strategy for the oxidative cleavage of C=C bonds in olefins using O_2 as the oxidant to form esters with one or multiple carbon atoms less was described using Co_{SA+NP}/N–C catalysts (Scheme 1a).[22] The Co_{SA} were the active centers for the Wacker-type oxidation of olefin, and Co_{NP} cleaved the C–C bonds in alcohols or ketones to form esters. Quinolines and quinazolinones were efficiently produced on a $Fe_3C_{NP}Fe_{NP}Fe_{SA}$/N–C catalyst *via* a cascade coupling process involving oxidative coupling of amines and aldehydes (Scheme 1b).[23] The catalyst consists in core-shell structured NPs with metallic and carbide iron NPs as the core and layers of graphitic carbon containing coordinated Fe–N_x SAs as the shell. Although the authors demonstrate that synergistic catalysis on SAs sites and NPs was primarily responsible for high activity and stability, no mechanism was proposed for that.

Electrocatalytic reactions usually involve multiple complex reaction steps. Co-electroreduction of CO_2 and water into synthesis gas was investigated on Ni_{SA+NP}/N–C catalysts, on which the SA/NP ratio was modulated *via* acid etching.[24] The Ni_{SA} show high selectivity towards the CO_2 reduction reaction (CO_2RR), while Ni_{NP} have preferential selectivity for the hydrogen evolution reaction (HER). Interestingly, it was possible to tune the CO/H_2 ratio of the syngas from 1:9 to 19:1 by controlling the Ni_{SA}/Ni_{NP} ratio in catalysts.

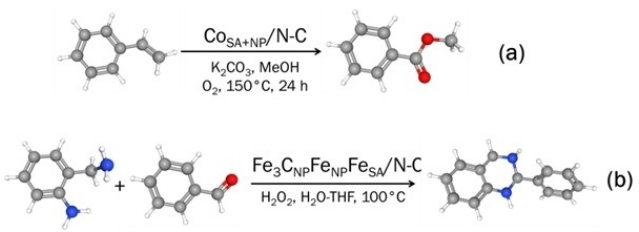

Scheme 1. Cascade reactions involving synergy between supported metal SAs and NPs: (**a**) oxidative cleavage of C=C bonds in olefins using O_2 as the oxidant to form esters;[20] and (**b**) oxidative coupling of amines and aldehydes to form quinazolinones.[21]

3. Synergistic Electronic Interaction

Synergistic effect due to (interfacial) electronic metal support interaction (EMSI) to enhance the catalytic performance has become a popular research strategy in electrocatalysis.[18b,c,25] Basically, the energy-level (*d*-band) regulation by electron transfer induced by the optimized structural configuration is shown to improve the charge transfer and separation behavior. Such type of interaction has to be considered for catalysts presenting a high loading (density) of metal SAs, which can modify the work function of the support but also altered the electronic structures of SAs themselves.[26] In highly diluted systems, the positive charge of the supported SAs originates from the bonds formed between the metal and support, leading to the electron transfer from the metal sites to the support. Compared with highly diluted systems that exhibit solely metal-support interactions, metal-metal interactions can appear in highly populated systems (correlated SACs), which can induce additional electronic effects *via* electron transfer between adjacent metal SAs.[27] Metal Organic Framework (MOF) pyrolysis often conducted to relative high SA density (both on the surface and embedded) and to the presence of metal clusters/NPs.[28] The support decorated with large amounts of metal SAs can be considered as a "modified support", which can improve metal NP stability.[29] The synergistic electronic interaction strategy has been used for many reactions in electrocatalysis.

The oxygen reduction reaction (ORR) both in acidic and basic media has been particularly studied since metal SAs (Co, Fe) in an MN_x environment (on N–C supports) are particularly attractive for this reaction.[30] For Fe_{SA+NP}/N–C catalysts, the active sites are the FeN_x SAs, Fe_{NP} being poorly active.[31] To understand the role that Fe_{NP} play in the experimentally evidenced superior ORR activity of Fe_{SA+NP}/N–C catalysts, DFT calculations are usually performed. The wide variety of models used, including Fe_{NP} on the support or on the Fe_{SA}, surely explains the differences in the levels of rationalization proposed from one study to another.[29b,30–32] According to the experimental results, the ORR proceeds *via* a four-electron pathway through O_2*, HOO*, O*, and HO* key intermediates. The explanation most often proposed is based on an electronic effect provided by the Fe_{NP} located near the isolated Fe atoms. The adjacent Fe_{NP} on the N-doped carbon support transfer electrons to the support. This contributes to an increase of the Fermi level about the whole system, meanwhile down-shifting the corresponding *d*-band center and lowering the binding strength of key ORR intermediates, hence enhancing both catalytic kinetics and thermodynamics. This is generally accompanied by an increase of the Bader charge on the metal SA.[32b,33] Increasing ORR activity was thus correlated to a decrease of the adsorption energy of one OH* intermediate,[29b,31,32b,d,34] or modification of energy barriers for OOH* formation or dissociation.[32a] Fe_{NP} were also proposed to increase the local charge density of FeN_4, subsequently enhancing O_2 adsorption/activation, resulting in the facile cleavage of the O–O bond.[30,32c] On N,P–C supports coloaded with Fe_{SA} and Fe_2P_{NP}, DFT calculations have shown that

phosphorous doping contribute to an upshifted *d*-band center of Fe, facilitating the adsorption of O_2. Thanks to the Fe_2P_{NP}, the active Fe_{SA} atom is in a low oxidation state and is less positively charged than in a Fe_{SA}/N,P–C catalyst, and serves as an electron reservoir capable of donating or releasing electrons, thereby improving the ORR activity.[35] It was also reported that in the presence of alloyed Pt_3M NPs (M=Fe, Zn), the Fe_{SA} immobilized on a N–C support are electrodeficient, resulting in a weaker adsorption strength of the OH* intermediate.[36] A decreased *d*-band center of Co atom for a Co_{SA+NP}/N–C system compared to its Co_{SA}/N–C counterpart was reported to affect the binding strength of key ORR intermediates (HOO*, O*).[37] Bimetallic systems such as $PtCo_{NP}Co_{SA}$/N–C[38] or $Co_{NP}Ru_{SA}$/N–C[39] were also reported.

The alkali hydrogen evolution reaction (HER) is a multistep reaction, of which the pathway is usually divided into three steps: H_2O splitting (Volmer step), the subsequent Heyrovsky desorption step, and H_2 desorption (Tafel step). A lowering of the *d*-band center of Ru for a $Ru_{NP}Co_{SA}$/O–C system compared to its Ru_{NP}/O–C counterpart (O–C: oxygen-doped graphene) due to EMSI was reported to result in a in weaker but more optimal H* binding strength for hydrogen evolution.[29a] A similar synergy was reported for a $Ru_{NP}Co_{SA}$/N–C catalyst (Figure 3a).[40] In that case, DFT calculation have shown that not only the Gibbs free energy (ΔG_{H^*}) decreases significantly when Ru_{NP} are associated to Co_{SA} ($\Delta G_{H^*} = -0.523$, -0.287 and -0.107 eV for N–C, Co_{SA}/N–C and $Ru_{NP}Co_{SA}$/N–C, respectively); but that the same tendency is observed for the energy barrier for H_2O dissociation (Figure 3b,c). Charge density distribution shows an enhanced hybridization of the Ru-*d* and Co-*d* orbitals, which is favorable for boosting interactions of dissociated intermediates at the Ru–Co coupling centers. Electron density difference mapping shows that the interaction of adsorbed H* is more favorable on Ru compared to the Co, N and C centers. This suggests that the synergy between Ru_{NP} and Co_{SA} can efficiently stimulate cleavage of the HO–H bonds to generate the H* species, which then adsorb at active Ru sites to boost the HER kinetic process. On pure ruthenium systems where Ru_{SA} and Ru_{NP} coexist on an N-doped carbon support, first-principles calculations have shown that Ru_{SA} present a much lower hydrogen binding energy than Ru_{NP},[41] and no discernable promotion of catalytic activity was observed for HER upon coloading of Ru_{SA} and Ru_{NP} on an N-doped carbon support.[42] Interestingly, when Ru_{SA} and Ru_{NP} are coloaded and in close proximity on a 3D crystalline fullerene network, a higher *d*-band center was measured for the Ru_{SA+NP}/C catalyst compared to Ru_{SA}/C or Ru_{NP}/C.[43] The higher *d*-band center was favorable towards water adsorption and further dissociation. In addition, the Ru_{SA+NP}/C catalyst facilitates the formation of H* and OH* intermediates. On a whole, the synergetic interaction between Ru_{SA} and Ru_{NP} reduced the reaction energy both from thermodynamic and kinetic viewpoint. Combining Co_4N_{NP} and Co_{SA} on N-doped CNTs also allows tailoring of the *d*-band center and Bader charges. In such system, the Co_{SA} provide the optimal value of 0.01 eV of ΔG_{H^*}.[44]

Platinum-based catalysts, including the ones containing mixtures of Pt_{SA} and Pt_{NP},[45] are generally considered to be the most effective electrocatalysts for the HER. On sulfur-doped TiN support, an optimized electronic structure of Pt for HER (thermodynamically favorable hydrogen adsorption free energy ΔG_{H^*}) was obtained when both Pt_{SA} and Pt_{NP} were present on the support.[46] On polymeric carbon nitride, the strong electronic interaction between Pt_{NP} (electron rich) and Pt_{SA} (electron deficient) tailors the 5d-band with a downward shift of the *d*-band center, resulting in an optimized H* binding strength compared to isolated Pt_{SA} or Pt_{NP}.[47] When Pt_{SA} or Pt_{NP} were deposited on a Co_{SA}/N–C support, the best configuration for an optimized ΔG_{H^*} was obtained with Pt_{NP}.[48]

Synergistic interactions resulting in a shift of the *d*-band center were also reported for the oxygen evolution reaction (OER) and overall water splitting. On $Co_{NP}Ir_{SA}$/N–C catalysts, the Ir_{SA} showed poor activity toward the OER, and Co_{NP} are the active sites.[49] Compared with the Co *d*-band center of -2.83 eV in Co_{NP}/N–C, the Co *d*-band center in $Co_{NP}Ir_{SA}$/N–C was upshifted to -2.22 eV. The upshift of the *d*-band center strengthened the binding of intermediates with Co_{NP} during OER. When the Ir_{SA} were located next to Co_{NP} (at a distance of 8.2 Å), the rate determining state (rds) transitioned from the formation of *OOH in Co_{NP}/N–C to the formation of *O. Moreover, the energy barrier of the rds was reduced from 1.81 eV on Co_{NP}/N–C to 1.72 eV on $Co_{NP}Ir_{SA}$/N–C. Chen *et al.* have proposed that integrating Cu_{SA} and Cu_{NP} on N-doped carbon in a single catalyst can not only adjust the sizes and metal loadings of Cu sites, but also regulate the local electron densities of Cu 3d orbitals, thereby contributing to rapid intermediate adsorption/desorption towards highly efficient water splitting.[50]

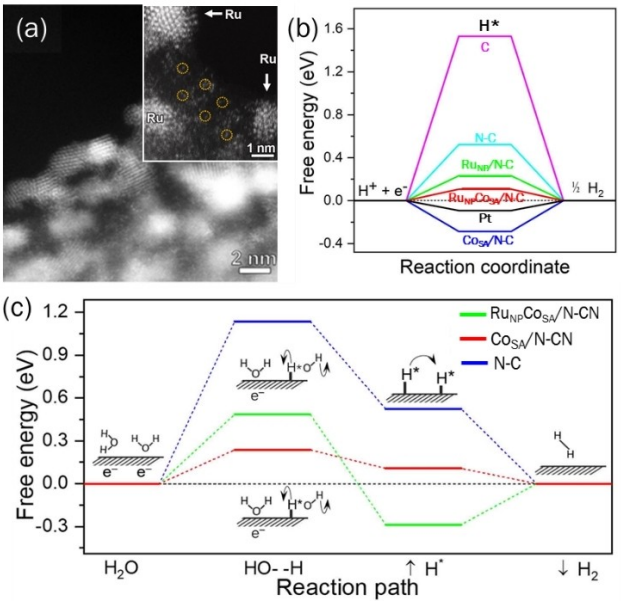

Figure 3. Synergistic interaction between Ru_{NP} and Co_{SA} for HER. (**a**) HAADF-STEM micrograph of a $Ru_{NP}Co_{SA}$/N–C electrocatalyst (5.36% w/w Ru; 0.84% w/w Co). (**b**) Calculated free energy diagram for HER on different surfaces; and (**c**) calculated energy diagram of the reaction path and corresponding mechanism at different stages of H_2O dissociation toward H_2 generation. Reprinted from ref.,[40] Copyright (2019), with permission from Elsevier.

In Li–CO_2 batteries, both CO_2RR ($4Li^+ + 3CO_2 + 4e^- \rightarrow 2Li_2CO_3 + C$) and CO_2 evolution reaction (CO_2ER; decomposition of Li_2CO_3 into Li^+ and CO_2) occur during the discharging and reverse charging process, respectively. On Ru_{SA+NP}/N–C catalysts, significant electron transfer between Ru_{SA} and Ru_{NP} was observed both experimentally and by modeling.[51] The Ru_{SA+NP}/N–C catalyst displays a lower work function than Ru_{SA}/N–C implying easier electron-emitting. The projected density of states of the Ru atom in Ru–N_4 sites in Ru_{SA+NP}/N–C and Ru_{SA}/N–C shows that both the *d*-band center and state density display significant difference, which verifies the electronic structure modulation for the Ru atom in Ru–N_4 sites by adjacent Ru_{NP}. The energy barriers for most sub-steps of CO_2RR (and CO_2ER) occurring on Ru_{SA} of Ru_{SA+NP}/N–C are lower than that occurring on Ru_{NP} as well as that occurring on Ru_{SA} of Ru_{SA}/N–C, suggesting that the Ru_{SA} should be the active site in the Ru_{SA+NP}/N–C catalyst. In this catalyst, the different interaction behavior between intermediate and the Ru_{SA} sites are essentially caused by the Ru_{NP} nearby.

Methanol[52] and ethanol[53] electrooxidation reactions were investigated on Pd-based catalysts deposited on carbon. Different synergistic interactions were evidenced according to the system investigated. On a N–C support, a mixture of Pd_{SA} and Pd_{NP} was used for methanol electrooxidation (MOR).[52] In that case, DFT calculation have shown that: i) the Pd_{SA} are not the active phase; ii) the *d*-band center of Pd_{NP} in Pd_{SA+NP}/N–C and Pd_{NP}/N–C catalysts are the same; and iii) the charge transfer is the key factor for the weakened binding strength with CO* species, suggesting a facile CO removal (improved CO poisoning resistance). So, in that case it is the EMSI between Pd_{SA} and the N-doped carbon support that boost the electron transfer at their interface, decreasing the charge transfer from Pd_{NP} to the support, thereby reducing the adsorption strength of CO on the Pd_{NP} and optimizing the MOR. When palladium-cobalt phosphide ($PdCo_2P$) NPs and Pd_{SA} were deposited on graphene oxide (GO) for ethanol electro-oxidation reaction (EOR) the EMSI results in a shift of the Pd *d*-band center that tailor the adsorption/desorption of reactants or intermediates, leading to an enhanced EOR performance.[53] Synergistic interaction between $PtZn_{NP}$ and Zn_{SA} immobilized on a N–C support was also reported for electrochemical ozone production.[54]

Synergistic electronic interactions between metal SAs and NPs were also reported in photocatalysis. Photocatalytic CO_2 reduction and C–C coupling to form ethylene was investigated on $AuCu_{NP}$-Cu_{SA}/TiO_2 catalysts.[55] The generation of photogenerated electrons and their migration to the surface to react with CO_2 are fundamental processes in photocatalytic CO_2RR. The photogenerated electrons promoted by $AuCu_{NP}$ under visible light are transferred to nearby Cu_{SA}, which can effectively promote the charge transfer and thus improve the photocatalytic activity for CO_2 reduction. Combined *in-situ* IR studies and DFT calculations have shown that compared to $AuCu_{NP}$/TiO_2 or Cu_{SA}/TiO_2 catalysts, the synergistic function of $AuCu_{NP}$ and Cu_{SA} enhances the adsorption and activation of CO_2 and H_2O, and lowers the overall activation energy barriers for C_2H_4 formation. Photocatalytic HER was investigated on Au_{SA+NP}/TiO_2 catalysts using a Na^+-modified defective TiO_2 support.[56] The reaction mainly consists of two steps: i) the photogenerated electrons reduce the adsorbed H^+ to produce H*; and ii) H* converts to H_2 and desorbs from the photocatalyst surface. A cascade electron transfer from Au_{NP} to TiO_2 and Au_{SA} for charge separation was evidenced. The Au_{NP} and Au_{SA} possess different affinities for electrons, inducing their different roles as electron donors and reservoirs during charge separation, respectively. The same reaction was studied on Pd_{SA+NP}/TiO_2 catalysts.[57] Theoretical calculations have shown that the synergistic effect of Pd_{NP} and Pd_{SA} can optimize the *d*-band center, and equilibrate the adsorption and desorption of intermediates during the reaction. The Pd_{NP} effectively promote the electron transfer to Pd_{SA} resulting in superior charge carrier separation efficiency. The Pd_{SA} is the active site that capture electrons to reduce H* into H_2.

Up to now, relatively few studies report synergistic electronic interactions in thermal catalysis. Zhang and coworkers employed such a strategy to regulate the chemoselectivity of a Pd catalyst for *p*-iodonitrobenzene hydrogenation.[58] Pd_{NP} and Zn_{SA} were coloaded on a O-doped carbon support coated on alumina. Three catalysts were tested: Pd_{NP}/O–C@Al_2O_3, Zn_{SA}/O–C@Al_2O_3, and $Pd_{NP}Zn_{SA}$/O–C@Al_2O_3. The Zn_{SA}/O–C@Al_2O_3 catalyst was not active. $Pd_{NP}Zn_{SA}$/O–C@Al_2O_3 is more active than Pd_{NP}/O–C@Al_2O_3 and shows high selectivity in hydrogenation of the iodo group rather than the nitro group in *p*-iodonitrobenzene to yield nitrobenzene. Density of states analyses show that the presence of Zn_{SA} move up the *d*-band center of Pd by approximately 0.94 eV, which accords with XANES analyses. For pure Pd_{NP}, *p*-iodonitrobenzene tends to adsorb on Pd atoms through both nitro and iodo groups, indicating that both two groups tend to be activated and hydrogenated. For Zn_{SA} inserted Pd_{NP}, the iodo group remains on Pd atoms where it can be hydrogenated, while the nitro group tends to interact with Zn_{SA}.

4. Synergy in Tandem or Binary Complementary Effect

For reactions where the active phase must activate dihydrogen, the cationic character of the SAs makes them clearly less active than the NPs. This is for example the case of alkene hydrogenation with Pd-supported catalysts, which is clearly favored over Pd_{NP}.[15b] However, it has been reported that cooperativity can function between Pd_{SA} and Pd_{NP} supported on carbon for the hydrogenation of alkenes.[59] The observed cooperativity involves: (i) the activation of H_2 on the Pd_{NP}, (ii) the spillover of hydrogen on the carbon support, which allows the formation of H–Pd_{SA} species, and (iii) the catalytic reaction on the H–Pd_{SA} species, which are much more active for hydrogenation than the H–Pd_{NP} species (Figure 4a).[59a] Even when a very small number of Pd_{NP} are present, the activity is quite different than the Pd_{SA} alone. This can be a common issue in studies aimed at examining solely the properties of SA in catalysts actually presenting a distribution of structures. A similar synergy was reported for other reducing agents such as $NaBH_4$ for 4-

Figure 4. Binary complementary effect for synergy in tandem with supported metal SAs and NPs. (**a**) H-spillover assisted cooperative catalysis between supported metal SAs and NPs for hydrogenation reactions. (**b**) Conversion of a LA/HMF mixtures to GVL and FDCA by synergistic catalysis between Ru_{SA} and Ru_{NP}.[68]

nitrophenol reduction on Pd_{SA+NP}/C catalysts,[60] or hydrazine on $Mo_{SA}MoO_{2\text{-}NP}$/N–C catalysts for transfer hydrogenation.[61] Interestingly, when using hydrazine as reducing agent on Fe_{SA}-$Fe_2O_{3\text{-}NP}$/N–C catalysts for selective reduction of nitro compounds, an opposite situation was observed. In that case, it is the Fe_{SA} that generate hydrogen by hydrazine decomposition and the nitrobenzene reduction to aniline is performed on $Fe_2O_{3\text{-}NP}$ surface.[62] In this type of cooperative catalysis, the best control for the balance between H_2 activation on NPs, H-spillover and the H-M_{SA} catalyzed hydrogenation rate involved a control of the NP/SA ratio[59a,63] and of support surface chemistry for optimized H-spillover. The generality of this type of synergy in hydrogenation or hydrodeoxygenation[64] has been demonstrated. It can involve metals other than palladium, such as Pt or Rh.[65] A wide variety of substrates such as ketones and aldehydes,[66] nitroaromatics,[67] CO_2,[20,63b] quinoline,[68] phenol derivatives[69] or alkynes can be (selectively) hydrogenated thanks to this cooperative catalysis.

Multiple reactions were also investigated. Thus, Ru_{SA+NP}/N–C catalysts were used for the hydrogenation of levulinic acid (LA) and the oxidation of 5-hydroxymethyl furfural (HMF).[70] The substrate mixture of LA and HMF was efficiently converted to the desired products γ-valerolactone (GVL) and 2,5-furandicarboxylic acid (FDCA) in a one-pot fashion (Figure 4b). The synergistic mechanism involved first H_2 dissociation over the Ru_{NP} surface and H-spillover from the Ru_{NP} to N atoms of the support. The formation of the N–H bond increases Ru_{SA} metallicity and strengthens LA adsorption. The Ru_{SA} perform better in LA hydrogenation than Ru_{NP}, and the product HPA also desorbs easily to the solvent and it is subsequently transforms to GVL through intramolecular esterification. The Ru_{NP} show also high activity in O_2 dissociation and HMF is adsorbed upon the Ru_{NP} surface to be oxidized to the final product FDCA.

In addition to carbon supports, other supports such as reducible oxides can be involved as long as they promote H-spillover.[66] When the metal SA is directly deposited on a metal NP, resulting in a single-atom alloy (SAA) catalyst, H-spillover occurs on the surface of the metal NP. This mechanism has been proposed for Pt_{SA}-Cu_{NP}[71] and Pd_{SA}-Cu_{NP}[72] systems that selectively promote the hydrogenation of C=O bonds in unsaturated aldehydes and alkynes, respectively, in which H_2 activation is proposed to occur on the noble metal SAs and hydrogenation on the surface of the NPs.

This type of synergy in tandem involving H-spillover is not limited to thermal catalysis and has been reported to be operative in electro- and photo-catalysis. Thus, for the alkaline HER on Pt_{SA+NP}/C catalysts, the Pt_{NP} are beneficial to water dissociation, while Pt_{SA} favor the H–H coupling into gaseous dihydrogen.[73] A similar behavior was also reported for photocatalytic HER on Pt_{SA+NP}/CdS and Pt_{SA+NP}/TiO_2 catalysts.[74]

On Ru_{SA}-RuO_{NP}/C catalysts, experimental and theoretical results suggest that the high HER electrocatalytic activity can be attributed to the following synergic catalytic pathway: i) first, H_2O is adsorbed on Ru_{SA}; then, ii) the oxygen of RuO_{NP} and the Ru_{SA} has strong binding affinity for hydrogen and hydroxyl groups, respectively, which accelerates water dissociation. Finally, H-spillover from RuO_{NP} to $Ru_{SA,}$ the Ru_{SA} has a weak hydrogen binding energy, promoting hydrogen desorption after .[75] Such mechanism, which also involved synergistic electronic interactions between Ru_{SA} and Ru_{NP} (electron transfer from Ru_{NP} to Ru_{SA}) was confirmed for various Ru_{SA+NP}/(N–)C catalysts.[43,76] The electrochemical reduction CO_2RR into value-added products by using clean energy and water (proton source) is a promising route toward carbon neutrality. Copper-based tandem electrocatalysts integrating Cu_{SA} and Cu_{NP} for CO_2-to-CO conversion have been reported.[77] For this reaction on Cu_{SA+NP}/N,S–C catalysts, Cu_{NP} catalyzed water dissociation and offered *H *via* H-spillover to the Cu_{SA}, which has an optimized binding energy for the key intermediate *COOH. The resulting *COOH intermediate was easily converted into *CO. The integration of Cu_{NP} adjacent to Cu_{SA} reduces the energy barrier of *COOH formation (synergistic electronic interaction). For the nitrogen reduction reaction (NRR) on $Mo_2C_{NP}Mo_{SA}$/CNT catalysts, DFT calculations have shown that the Mo_2C_{NP} are the active centers for N_2 production.[78] In that case, the Mo_{SA} are more selective for the HER reaction ($H^+ + e^- \rightarrow$ H*) and contribute to create an H*-rich microenvironment around the Mo_2C_{NP}, which is favorable for N_2 activation, and improve the overall selectivity and activity. Synergy between Pd_{SA} and Pd_{NP} *via* H-spillover was reported for enhancing CO_2 photoreduction to CH_4.[79] Mechanistic studies revealed that the Pd_{SA} activated the CO_2, while the Pd_{NP} boosted water dissociation for increased H* coverage. Proximity between Pd_{SA} and Pd_{NP} is required to stabilize intermediates such as *CHO, thereby favoring the pathway for CH_4 production.

This type of synergy involving spillover is not limited to H-spillover as shown for CO_2 methanation on various catalysts. On $Ru_{SA}Ni_{NP}$/CeO_2 catalysts, it was proposed that the Ru_{SA} converted

CO_2 to CO, while the Ni_{NP} were highly efficient for the subsequent CO methanation step.[80] For the CO_2RR on Cu_{SA+NP}/N–C catalysts, mechanistic analysis suggested that CO_2 is first reduced to CO over Cu_{SA}, followed by diffusion onto the neighboring Cu_{NP} for further reduction into CH_4.[81] On Cu_{SA+NP}/SiO_2 catalysts, the reverse water gas shift reaction (WGSR) was catalyzed by Cu_{NP}, while Cu_{SA} helped to inhibit CO desorption and further facilitate its hydrogenation to methanol.[82] For the WGSR on Cu_{SA+NP}/Al_2O_3 catalysts, Cu_{SA} strongly bind CO, and increase its concentration on catalyst surface to form a CO "pool" around Cu_{NP}, which are the active sites for the WGSR.[83] Single atom alloys have been shown to be highly selective for acetaldehyde production from ethanol dehydrogenation.[84] For ethanol dehydrogenation on NiCu SAAs, a spillover-mediated pathways from Ni_{SA} to Cu_{NP} of a hydroxyethyl intermediate (the dominant intermediate) was proposed based on microkinetic simulations. DFT studies coupled to kinetic and spectroscopic investigations have allowed to shed some light on the reaction mechanism. First, Ni_{SA} selectively activate ethanol by α-C–H bond scission (the rate-controlling step of the reaction) providing the 1-hydroxyethyl intermediate. After spillover of this intermediated from Ni_{SA} to Cu, the final O–H bond cleavage step to form acetaldehyde takes place over the Cu_{NP}.[85] For the EOR on $Pd_{NP}Ni_{SA}$/C catalysts, the Pd_{NP} catalyze the C–C bond breaking of ethanol, while the Ni_{SA} promote elimination of CO as CO_2.[86] This mechanism should involved CO spillover on the support. Spillover of hydroxyl was also proposed to rationalize the results obtained with $Co_{SA}PtCo_{NP}$/N–C catalyst for the photocatalytic overall water splitting without the use of any electron sacrificial agents.[87] The Co_{SA} are the active sites for H_2O activation and a spillover phenomenon of hydroxyl groups occurs between the Co_{SA} and the $PtCo_{NP}$. The Co_{SA} act as highly active sites for the HER half-reaction. Simultaneously, $PtCo_{NP}$ are configured to act as highly active sites for the OER.

When anchored on reducible oxides, some metal SAs greatly enhance the reducibility of the support and contribute to the generation of oxygen vacancies (O_v).[88] When NPs coexist with SAs in such systems, synergy in tandem can also operates. On Sn_{SA}-M_{NP}/TiO_2 catalysts (M=Au, Ru, Pt, Ni) used for the hydrogenation of nitroarenes, the Sn_{SA} contribute to the creation under the hydrogenation conditions of O_v on the TiO_2 surface; on which the nitro groups are adsorbed.[89] The nearby metal NPs activated H_2 and provided hydrogen atoms that facilitate both generation of O_v and nitroarene hydrogenation. On a Pd_{SA+NP}/TiO_2 catalyst used for water splitting coupled with selective oxidation of benzylamine to N-benzylidenebenzylamine, the electron transfer from Pd_{SA} to the support contributes to the stabilization of abundant O_v, which act as active sites for the adsorption and activation of H_2O and benzylamine.[90] Meanwhile, the Pd_{NP} promotes the photogenerated charge separation and provides the optimum sites for HER. The N-benzylidenebenzylamine is produced on the O_v by the condensation between benzylamine and an imine intermediate, which is formed during a multi-step mechanism involving the holes in TiO_2 as well OH^- and OH species. When anchored on non-reducible oxides such as zirconia, O_v can also be formed because of charge imbalance between cationic metal SAs and Zr^{4+} in the crystal lattice.[91] In ternary Pd–In_2O_3–ZrO_2 catalysts used for CO_2 hydrogenation to methanol, low-nuclearity palladium species were detected, among them Pd^{3+} species detected by EPR, indicating that Pd is strongly interacting with In_2O_3, likely replacing In^{3+} ions in the structure.[92] The remarkable methanol productivity of this catalyst was attributed to a higher density of O_v (likely stabilized by ZrO_2) on this ternary system compared to the binary counterparts. Further studies are needed to acquire detailed insights into the reaction mechanism on this ternary system.

Finally, synergy in tandem requiring high proximity between SAs and NPs was also observed for glycerol selective hydrogenation to glyceric acid on Pt_{SA+NP}/CeO_2[93] and Pt_{SA+NP}/Cu–$CuZrO_x$[16c] catalysts. In that case, some steps of the mechanism were proposed. First, the –OH bond activation occurred on the Pt_{NP} leading to the H abstraction. A C–H of glycerol was activated on the adjacent Pt_{SA}, which is the rate determining step. The cleavage of this C–H yielded propionaldehyde, which is adsorbed on the Pt_{NP} *via* its C=O bond, and the C–H of the aldehyde is reactivated by the Pt_{SA}. An oxygen is finally inserted in the activated C–H bond, forming glyceric acid.

5. Summary and Outlook

The absence of ensemble effects in SACs and the charge transfer to or from the support significantly affect the adsorption and induce a different reactivity compared to metallic NPs. This offers the possibility to have in SA-NP mixtures the same metal in two different oxidation states on the same support, which can be beneficial for some reactions. Bimetallic systems can also be considered. It emerges from this analysis on the work carried during the few last years that two types of cooperativities between SAs and NPs are generally proposed. The first type involves two-site catalysis (synergy in tandem and in parallel) with one type of chemical transformation occurring on SAs and another type on NPs. For the second (synergistic electronic interaction), the role of NPs is limited to modifying the electronic structure of SAs and *vice versa*, which leads to a modification of the reactivity. We of course suggest that the reader keep in mind that these two types of cooperativity could also coexist, particularly for highly loaded catalysts where synergistic electronic interaction have been evidenced. It is clear that this type of cooperative catalysis, which undoubtedly exists in many catalysts, opens up a large number of perspectives but also challenges (Figure 5). Once the possible synergy between supported SAs and NPs has been demonstrated for a given reaction and catalytic system, the question concerning their spatial distribution on the support but also the proportion of a type of species compared to the other must be asked. Indeed, these two fundamental characteristics of a system containing both metal SAs and NPs will have a profound influence on the extent of the synergy, and ultimately on the catalytic performance. The influence of the inter-site distance[94] or SA loading/density[26a,95] as well as of the SA/NP ratio[24,59a,63] on catalytic performance has already been demon-

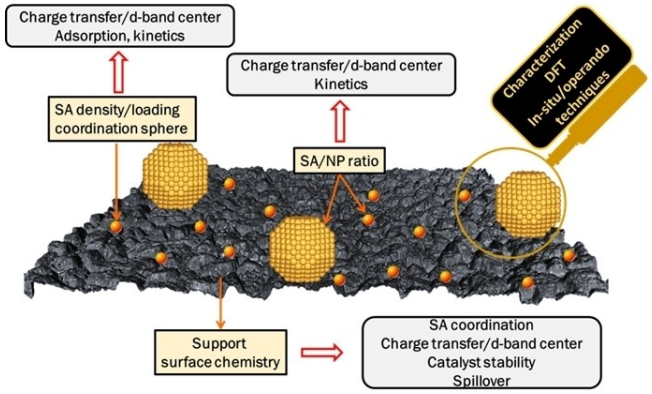

Figure 5. Main characteristics of a catalyst with a mixture of metal SAs and NPs to be considered and their impact on the catalytic performance.

strated in few studies dealing with monometallic systems. In that context, strategies are needed first to increase the density of metal SAs (if synergistic electronic interactions are aimed), while maintaining the homogeneity of the sites and avoiding the formation of any clusters or particles.[96] Additional work should be definitively performed to understand the effect of inter-SA distance in SACs for electro- but also photo- and thermal-catalysis. Second, synthetic strategies are also needed to prepare catalysts presenting similar metal loadings, similar NP size and controlled ratio of SAs and NPs to investigate synergy in tandem and in parallel. Considering the difficulty of this task, it might be interesting to use physical mixtures of pure metal SAC and pure supported NP catalyst.[19] Although in that case the communication between the species can be degraded since the two species are not on the same support, this approach offer the possibility to mix or not (dual beds of catalysts) the two species.

Another possibility will be to use a pure SAC and to add controlled amount of preformed NPs (colloidal NPs). Although this approach involved the use of ligands to stabilize the NPs, which can introduce some complexity in the system, it offers a high flexibility to control accurately the SA/NP ratio on the same support, while maintaining loading and NP size fixed. Although monometallic systems constitute most of the current literature on cooperative catalysis between SAs and NPs, the use of bimetallic systems has also been reported. Such an approach opens a vast chemical space for the discovery of new reactivity's and poses new challenges in terms of synthesis but also of characterization.

Fine characterization of catalysts containing mixtures of SAs and NPs (homo- or hetero-bimetallic) is highly challenging and deserves more studies. There are several techniques to analyze the distribution of metal SAs and NPs, including under realistic operating conditions.[8a,97] The first one is high-angle annular dark-field scanning transmission electron microscopy (HAADF-STEM), which allows probing supported SAs and NPs on an atomic scale, whether by Z-contrast imaging of structure, or by chemical analysis using energy dispersive X-ray spectroscopy (EDS), and electron energy loss spectroscopy (EELS). Such analyses require care to avoid electron beam damage to single-atom sites.

In addition, microscopy is a local probe, and other techniques can be used to confirm the STEM results while analyzing a significant amount of the produced catalysts. These techniques are X-ray absorption spectroscopy (XAS), X-ray Photoelectron Spectroscopy (XPS) and Diffuse Reflectance Fourier Transform Infrared Spectroscopy (DRIFTS), which all present some limitations. DRIFTS provides chemical and structural information related to surface species and on occupancies of the metal d states, commonly through measurement of adsorbed probe molecules (e.g., CO). However, DRIFTS is not possible on carbon materials because they absorb most of the IR radiation. On oxide supports, the presence of multiple speciation in samples containing both SAs and clusters may complicate the interpretation of the spectroscopic data. In that context, complementary XAS analyses assisted by DFT can be helpful.[98]

XAS is a popular technique for SAC characterization,[99] which allows extracting electronic and geometric structural information and that is well adapted for samples containing only SAs or only NPs. When mixtures of SAs and NPs are present this method shows some limitations.[100] It should be noted that EXAFS is more sensitive to heavier elements, than lighter ones, which means that the metal-metal distances in the NPs will dominate the results. When analyzing mixtures of SAs and NPs, EXAFS is not sensitive enough to identify SAs, which may easily confuse the contributions from small clusters or NPs due to the polydispersity and disorder effects. In addition, it has been shown that EXAFS is not capable of unambiguously identifying the co-existence of oxidized or even metallic NPs as minority species in samples containing predominantly SAs, yet such minority species may often contribute to the catalytic behavior.[100b]

XPS is a widely used surface-sensitive quantitative technique to probe the chemical and compositional properties of solid surfaces and to determine the surface electronic structures. In XPS, semi-quantitative determination of a SA/NP ratio can be difficult in samples with a significant amount of clusters that present, as SAs, significant charge transfer with the support.[101] The situation becomes even more difficult when it is necessary to characterize heterobimetallic systems. Indeed, in this case and because of the synthetic routes used, it is possible that the SAs are located not only on the support but also on the surface of the NPs of the second metal (SAA type). It will then also be necessary to study the possible synergy between these different species/situations. It is important to keep all these difficulties in mind when characterizing these complex systems containing metal sites ranging from NPs to clusters and SAs that definitively required the use of the complimentary characterization techniques discussed above, but also of others such as solid-state nuclear magnetic resonance (ss-NMR),[102] or Mossbauer spectroscopy.[103] An alternative to multiple characterization techniques, which has been rarely examined, consist in studying structure sensitive catalytic reactions (reaction testing direct strategy).[14,101,104] Owing to different reaction mechanisms/kinetics on SAs and NPs, reaction kinetics can

serve as a surface sensitive characterization tool for quantifying their surface site fractions.

It is also worth noting that all studies relating to the cooperativity between SAs and NPs are essentially based on catalytic results, often coupled with modelling studies. The rationality of theoretical modeling shall be consistent with the actual characterization results, and great care should be taken in the choice of a realistic model. This is a crucial point for the rationalization of catalytic results, which is often based on DFT, as we have seen in the case of Fe_{SA+NP}/N–C catalysts for ORR. Finally, if we consider that the proposed synergies constitutes possibly only one explanation among others for the catalytic performances (e.g. coordination sphere of SAs, size of metal NPs, distance between SAs and NPs…), it is important to carry out, in complement of DFT calculations[105] and machine learning tool use,[106] *operando/in-situ* studies on such complex systems to support the hypotheses put forward, as it has already been done in the case of SACs.[97e]

Acknowledgements

This work was supported by the Agence Nationale de la Recherche (ANR-19-CE07-0030, COMET), which is gratefully acknowledged.

Conflict of Interests

The author declares no conflict of interest.

Data Availability Statement

Data sharing is not applicable to this article as no new data were created or analyzed in this study.

Keywords: supported catalysts · single atoms · nanoparticles · charge transfer · spillover

[1] D. Pham Minh, P. Serp, *in Supported Metal Single Atom Catalysis* (eds P. Serp and D.P. Minh) **2022**, pp. 1–49.
[2] P. Kalck, C. Le Berre, P. Serp, *Coord. Chem. Rev.* **2020**, *402*, 213078.
[3] S. Mitchell, J. Pérez-Ramírez, *Nat. Commun.* **2020**, *11*, 4302.
[4] a) J.-C. Liu, Y. Tang, Y.-G. Wang, T. Zhang, J. Li, *Natl. Sci. Rev.* **2018**, *5*, 638–641; b) Y.-Q. Su, L. Zhang, Y. Wang, J.-X. Liu, V. Muravev, K. Alexopoulos, I. A. W. Filot, D. G. Vlachos, E. J. M. Hensen, *npj Comput. Mater.* **2020**, *6*, 144.
[5] T. Iwasawa, M. Tokunaga, Y. Obora, Y. Tsuji, *J. Am. Chem. Soc.* **2004**, *126*, 6554–6555.
[6] L. Liu, A. Corma, *Trends Chem.* **2020**, *2*, 383–400.
[7] a) D. O. Prima, N. S. Kulikovskaya, A. S. Galushko, R. M. Mironenko, V. P. Ananikov, *Curr. Opin. Green Sustain. Chem.* **2021**, *31*, 100502; b) V. P. Ananikov, I. P. Beletskaya, *Organometallics* **2012**, *31*, 1595–1604.
[8] a) E. C. Tyo, S. Vajda, *Nat. Nanotechnol.* **2015**, *10*, 577–588; b) W. E. Kaden, T. Wu, W. A. Kunkel, S. L. Anderson, *Science* **2009**, *326*, 826–829; c) Z. Zhang, B. Zandkarimi, A. N. Alexandrova, *Acc. Chem. Res.* **2020**, *53*, 447–458.
[9] a) P. L. Gai, L. Lari, M. R. Ward, E. D. Boyes, *Chem. Phys. Lett.* **2014**, *592*, 355–359; b) E. D. Boyes, A. P. LaGrow, M. R. Ward, R. W. Mitchell, P. L. Gai, *Acc. Chem. Res.* **2020**, *53*, 390–399.
[10] a) J.-C. Liu, Y.-G. Wang, J. Li, *J. Am. Chem. Soc.* **2017**, *139*, 6190–6199; b) Y.-G. Wang, D. Mei, V.-A. Glezakou, J. Li, R. Rousseau, *Nat. Commun.* **2015**, *6*, 6511; c) C. Schilling, M. Ziemba, C. Hess, M. V. Ganduglia-Pirovano, *J. Catal.* **2020**, *383*, 264–272.
[11] G. Lan, Q. Ye, Y. Zhu, H. Tang, W. Han, Y. Li, *ACS Appl. Nano Mater.* **2020**, *3*, 3004–3010.
[12] V. I. Bukhtiyarov, M. G. Slin'ko, *Russ. Chem. Rev.* **2001**, *70*, 147–159.
[13] Y. Guo, M. Wang, Q. Zhu, D. Xiao, D. Ma, *Nature Catal.* **2022**, *5*, 766–776.
[14] G. D. Lei, W. M. H. Sachtler, *J. Catal.* **1993**, *140*, 601–611.
[15] a) Y. Deng, Y. Guo, Z. Jia, J.-C. Liu, J. Guo, X. Cai, C. Dong, M. Wang, C. Li, J. Diao, Z. Jiang, J. Xie, N. Wang, H. Xiao, B. Xu, H. Zhang, H. Liu, J. Li, D. Ma, *J. Am. Chem. Soc.* **2022**, *144*, 3535–3542; b) M. D. Rossell, F. J. Caparrós, I. Angurell, G. Muller, J. Llorca, M. Seco, O. Rossell, *Catal. Sci. Technol.* **2016**, *6*, 4081–4085.
[16] a) M. Cui, Q. Qian, J. Zhang, Y. Wang, B. B. Asare Bediako, H. Liu, B. Han, *Chem* **2021**, *7*, 726–737; b) J. Sun, H. Li, H. Huang, B. Wang, L.-P. Xiao, G. Song, *ChemSusChem* **2018**, *11*, 1157–1162; c) M. Wang, Z. Zhao, C. Li, H. Li, J. Liu, Q. Yang, *Nat. Commun.* **2022**, *13*, 5699.
[17] U. Petek, F. Ruiz-Zepeda, M. Bele, M. Gaberšček, *Catalysts* **2019**, *9*, 134.
[18] a) P. Serp, *Nanoscale* **2021**, *13*, 5985–6004; b) L. Zhang, J. Zhu, X. Li, S. Mu, F. Verpoort, J. Xue, Z. Kou, J. Wang, *Interdiscip. Mater.* **2022**, *1*, 51–87; c) W. Xu, M. Cao, J. Luo, H. Mao, H. Gu, Z. Sun, Q. Liu, S. Zhang, *Mater. Chem. Front.* **2023**, *7*, 1992–2013.
[19] C. B. Thompson, Y. Lu, A. M. Karim, *Ind. Eng. Chem. Res.* **2021**, *60*, 15960–15971.
[20] B. Wang, M. Li, S. Zhang, H. Wu, Y. Liao, H. Li, *Appl. Catal. B* **2023**, *327*, 122454.
[21] J. Zhang, M. Wang, Z. Gao, X. Qin, Y. Xu, Z. Wang, W. Zhou, D. Ma, *J. Am. Chem. Soc.* **2022**, *144*, 5108–5115.
[22] X. Yu, Z. Zhao, S. Tan, L. Zhu, W. Fu, Y. An, L. Wang, *Chem. Commun.* **2021** https://doi.org/10.1039/D1CC01596F.
[23] Z. Ma, T. Song, Y. Yuan, Y. Yang, *Chem. Sci.* **2019**, *10*, 10283–10289.
[24] W. Zhu, J. Fu, J. Liu, Y. Chen, X. Li, K. Huang, Y. Cai, Y. He, Y. Zhou, D. Su, J.-J. Zhu, Y. Lin, *Appl. Catal. B* **2020**, *264*, 118502.
[25] T. Dong, J. Ji, L. Yu, P. Huang, Y. Li, Z. Suo, B. Liu, Z. Hu, H. Huang, *JACS Au* **2023**, *3*, 1230–1240.
[26] a) H. Jin, P. Cui, C. Cao, X. Yu, R. Zhao, D. Ma, W. Song, *ACS Catal.* **2023**, *13*, 1316–1325; b) J. Yang, W. Li, D. Wang, Y. Li, *Adv. Mater.* **2020**, *32*, 2003300; c) K. Qi, M. Chhowalla, D. Voiry, *Mater. Today* **2020**, *40*, 173–192.
[27] J. Shan, C. Ye, Y. Jiang, M. Jaroniec, Y. Zheng, S.-Z. Qiao, *Sci. Adv.* **2022**, *8*, eabo0762.
[28] S. Ma, W. Han, W. Han, F. Dong, Z. Tang, *J. Mater. Chem. A* **2023**, *11*, 3315–3363.
[29] a) P. Su, W. Pei, X. Wang, Y. Ma, Q. Jiang, J. Liang, S. Zhou, J. Zhao, J. Liu, G. Q. Lu, *Angew. Chem. Int. Ed.* **2021**, *60*, 16044–16050; b) L. Li, Y. Wen, G. Han, F. Kong, L. Du, Y. Ma, P. Zuo, C. Du, G. Yin, *Small* **2023**, 2300758.
[30] W.-J. Jiang, L. Gu, L. Li, Y. Zhang, X. Zhang, L.-J. Zhang, J.-Q. Wang, J.-S. Hu, Z. Wei, L.-J. Wan, *J. Am. Chem. Soc.* **2016**, *138*, 3570–3578.
[31] X. Ao, W. Zhang, Z. Li, J.-G. Li, L. Soule, X. Huang, W.-H. Chiang, H. M. Chen, C. Wang, M. Liu, X. C. Zeng, *ACS Nano* **2019**, *13*, 11853–11862.
[32] a) S.-N. Zhao, J.-K. Li, R. Wang, J. Cai, S.-Q. Zang, *Adv. Mater.* **2022**, *34*, 2107291; b) H. Huang, D. Yu, F. Hu, S.-C. Huang, J. Song, H.-Y. Chen, L. L. Li, S. Peng, *Angew. Chem. Int. Ed.* **2022**, *61*, e202116068; c) S.-H. Yin, J. Yang, Y. Han, G. Li, L.-Y. Wan, Y.-H. Chen, C. Chen, X.-M. Qu, Y.-X. Jiang, S.-G. Sun, *Angew. Chem. Int. Ed.* **2020**, *59*, 21976–21979; d) X. Wan, Q. Liu, J. Liu, S. Liu, X. Liu, L. Zheng, J. Shang, R. Yu, J. Shui, *Nat. Commun.* **2022**, *13*, 2963.
[33] J. Zhang, Y. Xie, Q. Jiang, S. Guo, J. Huang, L. Xu, Y. Wang, G. Li, *J. Mater. Chem. A* **2022**, *10*, 16920–16927.
[34] M. Chen, F. Kong, H. Yao, Y. Chen, G. Meng, Z. Chang, C. Chen, H. Tian, L. Wang, X. Cui, J. Shi, *Chem. Eng. J.* **2023**, *453*, 139820.
[35] Y. Pan, X. Ma, M. Wang, X. Yang, S. Liu, H.-C. Chen, Z. Zhuang, Y. Zhang, W.-C. Cheong, C. Zhang, X. Cao, R. Shen, Q. Xu, W. Zhu, Y. Liu, X. Wang, X. Zhang, W. Yan, J. Li, H. M. Chen, C. Chen, Y. Li, *Adv. Mater.* **2022**, *34*, 2203621.
[36] X. Ao, W. Zhang, B. Zhao, Y. Ding, G. Nam, L. Soule, A. Abdelhafiz, C. Wang, M. Liu, *Energy Environ. Sci.* **2020**, *13*, 3032–3040.
[37] W. Zhou, H. Su, Z. Wang, F. Yu, W. Wang, X. Chen, Q. Liu, *J. Mater. Chem. A* **2021**, *9*, 1127–1133.
[38] L. Chong, J. Wen, J. Kubal, F. G. Sen, J. Zou, J. Greeley, M. Chan, H. Barkholtz, W. Ding, D.-J. Liu, *Science* **2018**, *362*, 1276–1281.

[39] Z. Liu, S. Zhou, S. Ma, J. Li, Z. Yang, H. Cheng, W. Cai, *Mater. Today Phys.* **2021**, *17*, 100338.
[40] S. Yuan, Z. Pu, H. Zhou, J. Yu, I. S. Amiinu, J. Zhu, Q. Liang, J. Yang, D. He, Z. Hu, G. Van Tendeloo, S. Mu, *Nano Energy* **2019**, *59*, 472–480.
[41] B. Lu, L. Guo, F. Wu, Y. Peng, J. E. Lu, T. J. Smart, N. Wang, Y. Z. Finfrock, D. Morris, P. Zhang, N. Li, P. Gao, Y. Ping, S. Chen, *Nat. Commun.* **2019**, *10*, 631.
[42] R. Ma, X. Wang, X. Yang, Y. Li, C. Liu, J. Ge, W. Xing, *Nano Res.* **2023**, *16*, 166–173.
[43] T. Luo, J. Huang, Y. Hu, C. Yuan, J. Chen, L. Cao, K. Kajiyoshi, Y. Liu, Y. Zhao, Z. Li, Y. Feng, *Adv. Funct. Mater.* **2023**, *33*, 2213058.
[44] B. Cao, M. Hu, Y. Cheng, P. Jing, B. Liu, B. Zhou, X. Wang, R. Gao, X. Sun, Y. Du, J. Zhang, *NPG Asia Mater.* **2021**, *13*, 1.
[45] a) N. Cheng, S. Stambula, D. Wang, M. N. Banis, J. Liu, A. Riese, B. Xiao, R. Li, T.-K. Sham, L.-M. Liu, G. A. Botton, X. Sun, *Nat. Commun.* **2016**, *7*, 13638; b) J. N. Tiwari, S. Sultan, C. W. Myung, T. Yoon, N. Li, M. Ha, A. M. Harzandi, H. J. Park, D. Y. Kim, S. S. Chandrasekaran, W. G. Lee, V. Vij, H. Kang, T. J. Shin, H. S. Shin, G. Lee, Z. Lee, K. S. Kim, *Nat. Energy* **2018**, *3*, 773–782.
[46] J. Yan, Z. Xi, L. Cong, K. Lv, R. Xin, B. Cao, B. Liu, J. He, J. Zhang, *Small* **2022**, *18*, 2205603.
[47] M. Gao, F. Tian, Z. Guo, X. Zhang, Z. Li, J. Zhou, X. Zhou, Y. Yu, W. Yang, *Chem. Eng. J.* **2022**, *446*, 137127.
[48] Y. Zhao, P. V. Kumar, X. Tan, X. Lu, X. Zhu, J. Jiang, J. Pan, S. Xi, H. Y. Yang, Z. Ma, T. Wan, D. Chu, W. Jiang, S. C. Smith, R. Amal, Z. Han, X. Lu, *Nat. Commun.* **2022**, *13*, 2430.
[49] X. Ding, C. Jia, P. Ma, H. Chen, J. Xue, D. Wang, R. Wang, H. Cao, M. Zuo, S. Zhou, Z. Zhang, J. Zeng, J. Bao, *Nano Lett.* **2023**, *23*, 3309–3316.
[50] W. Zhang, R. Liu, Z. Fan, H. Wen, Y. Chen, R. Lin, Y. Zhu, X. Yang, Z. Chen, *Inorg. Chem. Front.* **2023**, *10*, 443–453.
[51] J. Lin, J. Ding, H. Wang, X. Yang, X. Zheng, Z. Huang, W. Song, J. Ding, X. Han, W. Hu, *Adv. Mater.* **2022**, *34*, 2200559.
[52] L. Zhuang, Z. Jia, Y. Wang, X. Zhang, S. Wang, J. Song, L. Tian, T. Qi, *Chem. Eng. J.* **2022**, *438*, 135585.
[53] J. N. Tiwari, N. K. Dang, H. J. Park, S. Sultan, M. G. Kim, J. Haiyan, Z. Lee, K. S. Kim, *Nano Energy* **2020**, *78*, 105166.
[54] B. Yuan, Z. Yao, C. Qiu, H. Zheng, Y. Yan, Q. Zhang, X. Sun, Y. Gu, X. Zhong, J. Wang, *J. Energy Chem.* **2020**, *51*, 312–322.
[55] Y. Yu, X. A. Dong, P. Chen, Q. Geng, H. Wang, J. Li, Y. Zhou, F. Dong, *ACS Nano* **2021**, *15*, 14453–14464.
[56] X. An, T. Wei, P. Ding, L.-M. Liu, L. Xiong, J. Tang, J. Ma, F. Wang, H. Liu, J. Qu, *J. Am. Chem. Soc.* **2023**, *145*, 1759–1768.
[57] T. Lv, B. Xiao, F. Xia, M. Chen, J. Zhao, Y. Ma, J. Wu, J. Zhang, Y. Zhang, Q. Liu, *Chem. Eng. J.* **2022**, *450*, 137873.
[58] S.-S. Zhang, J. Yi, T. Cao, J.-P. Guan, J.-Q. Sun, Q.-Y. Zhao, Y.-J. Qiu, C.-L. Ye, Y. Xiong, G. Meng, W. Chen, Z. Lin, J. Zhang, *Small* **2023**, *19*, 2206052.
[59] a) C. Rivera-Cárcamo, I. C. Gerber, I. del Rosal, B. Guicheret, R. Castro Contreras, L. Vanoye, A. Favre-Réguillon, B. F. Machado, J. Audevard, C. de Bellefon, R. Philippe, P. Serp, *Catal. Sci. Technol.* **2021**, *11*, 984–999; b) B. Guicheret, L. Vanoye, C. Rivera-Cárcamo, C. de Bellefon, P. Serp, R. Philippe, A. Favre-Réguillon, *ChemSusChem* **2022**, *15*, e202200916; c) L. Vanoye, B. Guicheret, C. Rivera-Cárcamo, R. Castro Contreras, C. de Bellefon, V. Meille, P. Serp, R. Philippe, A. Favre-Réguillon, *Chem. Eng. J.* **2022**, *441*, 135951.
[60] J. Audevard, A. Benyounes, R. Castro Contreras, H. Abou Oualid, M. Kacimi, P. Serp, *ChemCatChem* **2022**, *14*, e202101783.
[61] Z.-N. Hu, Y. Ai, Y. Zhao, Y. Wang, K. Ding, W. Zhang, R. Guo, X. Zhang, X. Cai, N. Wang, J. Hu, Q. Liang, H. Liu, F. Huang, L. Wu, J. Zhang, H.-b. Sun, *Nano Res.* **2023**, *16*, 2302–2310.
[62] R. Yun, F. Zhan, N. Li, B. Zhang, W. Ma, L. Hong, T. Sheng, L. Du, B. Zheng, S. Liu, *ACS Appl. Mater. Interfaces* **2020**, *12*, 34122–34129.
[63] a) S. Shao, Z. Ding, C. Shang, S. Zhang, Y. Ke, G. Zhu, Y. Yang, *Chem. Eng. J.* **2022**, *450*, 138153; b) E. H. Kim, M. H. Lee, J. Kim, E. C. Ra, J. H. Lee, J. S. Lee, *Chin. J. Catal.* **2023**, *47*, 214–221.
[64] X. Lu, C. Guo, M. Zhang, L. Leng, J. H. Horton, W. Wu, Z. Li, *Nano Res.* **2021**, *14*, 4347–4355.
[65] J. Yang, L. Yang, L. Zhang, T. Yu, D. Zhai, H. Wang, W. Zhou, Y. Li, G. Ren, L. Sun, W. Deng, *Chem. - Eur. J.* **2023**, *29*, e202203108.
[66] L. Kuai, Z. Chen, S. Liu, E. Kan, N. Yu, Y. Ren, C. Fang, X. Li, Y. Li, B. Geng, *Nat. Commun.* **2020**, *11*, 48.
[67] L. Zhu, Y. Sun, H. Zhu, G. Chai, Z. Yang, C. Shang, H. Ye, B. H. Chen, A. Kroner, Z. Guo, *ACS Catal.* **2022**, *12*, 8104–8115.
[68] Q. Shen, H. Jin, P. Li, X. Yu, L. Zheng, W. Song, C. Cao, *Nano Res.* **2022**, *15*, 5024–5031.
[69] B. Wang, P. Zhou, X. Yan, H. Li, H. Wu, Z. Zhang, *J. Energy Chem.* **2023**, *79*, 535–549.
[70] L. Zhang, G. Meng, W. Zhang, X. Li, Z. Zhang, M. Yang, Y. Wu, D. Wang, Y. Li, *ACS Catal.* **2023**, *13*, 2268–2276.
[71] Y. Cao, J. Guerrero-Sańchez, I. Lee, X. Zhou, N. Takeuchi, F. Zaera, *ACS Catal.* **2020**, *10*, 3431–3443.
[72] L. Jiang, K. Liu, S.-F. Hung, L. Zhou, R. Qin, Q. Zhang, P. Liu, L. Gu, H. M. Chen, G. Fu, N. Zheng, *Nat. Nanotechnol.* **2020**, *15*, 848–853.
[73] a) Y. Zhu, P. Tian, H. Jiang, J. Mu, L. Meng, X. Su, Y. Wang, Y. Lin, Y. Zhu, L. Song, C. Li, *CCS Chemistry* **2021**, *3*, 2539–2547; b) C. Wang, F. Chen, Q. Wang, X. Yang, H. Zang, N. Yu, B. Geng, *Carbon* **2023**, *201*, 278–284.
[74] J. Zhang, Y. Pan, D. Feng, L. Cui, S. Zhao, J. Hu, S. Wang, Y. Qin, *Adv. Mater.* **2023**, *38*, 2300902.
[75] D. Cao, J. Wang, H. Xu, D. Cheng, *Small* **2021**, *17*, 2101163.
[76] a) Q. Hu, G. Li, X. Huang, Z. Wang, H. Yang, Q. Zhang, J. Liu, C. He, *J. Mater. Chem. A* **2019**, *7*, 19531–19538; b) S. Wang, M. Wang, Z. Liu, S. Liu, Y. Chen, M. Li, H. Zhang, Q. Wu, J. Guo, X. Feng, Z. Chen, Y. Pan, *ACS Appl. Mater. Interfaces* **2022**, *14*, 15250–15258.
[77] D. Chen, L.-H. Zhang, J. Du, H. Wang, J. Guo, J. Zhan, F. Li, F. Yu, *Angew. Chem. Int. Ed.* **2021**, *60*, 24022–24027.
[78] Y. Ma, T. Yang, H. Zou, W. Zang, Z. Kou, L. Mao, Y. Feng, L. Shen, S. J. Pennycook, L. Duan, X. Li, J. Wang, *Adv. Mater.* **2020**, *32*, 2002177.
[79] P. Liu, Z. Huang, X. Gao, X. Hong, J. Zhu, G. Wang, Y. Wu, J. Zeng, X. Zheng, *Adv. Mater.* **2022**, *34*, 2200057.
[80] T. Zhang, P. Zheng, F. Gu, W. Xu, W. Chen, T. Zhu, Y.-F. Han, G. Xu, Z. Zhong, F. Su, *Appl. Catal. B* **2023**, *323*, 122190.
[81] Q. Zhao, Y. Wang, M. Li, S. Zhu, T. Li, J. Yang, T. Lin, E. P. Delmo, Y. Wang, J. Jang, M. Gu, M. Shao, *SmartMat* **2022**, *3*, 183–193.
[82] J. Yu, M. Yang, J. Zhang, Q. Ge, A. Zimina, T. Pruessmann, L. Zheng, J.-D. Grunwaldt, J. Sun, *ACS Catal.* **2020**, *10*, 14694–14706.
[83] Z. Cui, S. Song, H. Liu, Y. Zhang, F. Gao, T. Ding, Y. Tian, X. Fan, X. Li, *Appl. Catal. B* **2022**, *313*, 121468.
[84] a) J. Shan, N. Janvelyan, H. Li, J. Liu, T. M. Egle, J. Ye, M. M. Biener, J. Biener, C. M. Friend, M. Flytzani-Stephanopoulos, *Appl. Catal. B* **2017**, *205*, 541–550; b) G. Giannakakis, A. Trimpalis, J. Shan, Z. Qi, S. Cao, J. Liu, J. Ye, J. Biener, M. Flytzani-Stephanopoulos, *Top. Catal.* **2018**, *61*, 475–486; c) J. Shan, J. Liu, M. Li, S. Lustig, S. Lee, M. Flytzani-Stephanopoulos, *Appl. Catal. B* **2018**, *226*, 534–543; d) M. Ouyang, K. G. Papanikolaou, A. Boubnov, A. S. Hoffman, G. Giannakakis, S. R. Bare, M. Stamatakis, M. Flytzani-Stephanopoulos, E. C. H. Sykes, *Nat. Commun.* **2021**, *12*, 1549.
[85] D. A. Patel, G. Giannakakis, G. Yan, H. T. Ngan, P. Yu, R. T. Hannagan, P. L. Kress, J. Shan, P. Deshlahra, P. Sautet, E. C. H. Sykes, *ACS Catal.* **2023**, *13*, 4290–4303.
[86] S. Li, A. Guan, H. Wang, Y. Yan, H. Huang, C. Jing, L. Zhang, L. Zhang, G. Zheng, *J. Mater. Chem. A* **2022**, *10*, 6129–6133.
[87] B.-B. Xu, X.-B. Fu, X.-M. You, E. Zhao, F.-F. Li, Z. Chen, Y.-X. Li, X. L. Wang, Y.-F. Yao, *ACS Catal.* **2022**, *12*, 6958–6967.
[88] a) J. Lin, A. Wang, B. Qiao, X. Liu, X. Yang, X. Wang, J. Liang, J. Li, J. Liu, T. Zhang, *J. Am. Chem. Soc.* **2013**, *135*, 15314–15317; b) L. Nie, D. Mei, H. Xiong, B. Peng, Z. Ren, X. I. P. Hernandez, A. DeLaRiva, M. Wang, M. H. Engelhard, L. Kovarik, A. K. Datye, Y. Wang, *Science* **2017**, *358*, 1419–1423.
[89] L. Wang, E. Guan, J. Zhang, J. Yang, Y. Zhu, Y. Han, M. Yang, C. Cen, G. Fu, B. C. Gates, F.-S. Xiao, *Nat. Commun.* **2018**, *9*, 1362.
[90] T. Wang, X. Tao, X. Li, K. Zhang, S. Liu, B. Li, *Small* **2021**, *17*, 2006255.
[91] N. H. M. D. Dostagir, R. Rattanawan, M. Gao, J. Ota, J.-Y. Hasegawa, K. Asakura, A. Fukouka, A. Shrotri, *ACS Catal.* **2021**, *11*, 9450–9461.
[92] T. Pinheiro Araújo, C. Mondelli, M. Agrachev, T. Zou, P. O. Willi, K. M. Engel, R. N. Grass, W. J. Stark, O. V. Safonova, G. Jeschke, S. Mitchell, J. Pérez-Ramírez, *Nat. Commun.* **2022**, *13*, 5610.
[93] Z. Luo, Z. Zhu, R. Xiao, D. Chu, *ChemNanoMat* **2023**, *9*, e202200494.
[94] a) Z. Jin, P. Li, Y. Meng, Z. Fang, D. Xiao, G. Yu, *Nature Catal.* **2021**, *4*, 615–622; b) B. Wang, C. Cheng, M. Jin, J. He, H. Zhang, W. Ren, J. Li, D. Wang, Y. Li, *Angew. Chem. Int. Ed.* **2022**, *61*, e202207268.
[95] a) C. Xia, Y. Qiu, Y. Xia, P. Zhu, G. King, X. Zhang, Z. Wu, J. Y. Kim, D. A. Cullen, D. Zheng, P. Li, M. Shakouri, E. Heredia, P. Cui, H. N. Alshareef, Y. Hu, H. Wang, *Nat. Chem.* **2021**, *13*, 887–894; b) X. Hai, S. Xi, S. Mitchell, K. Harrath, H. Xu, D. F. Akl, D. Kong, J. Li, Z. Li, T. Sun, H. Yang, Y. Cui, C. Su, X. Zhao, J. Li, J. Pérez-Ramírez, J. Lu, *Nat. Nanotechnol.* **2022**, *17*, 174–181; c) H. Jin, R. Zhao, P. Cui, X. Liu, J. Yan, X. Yu, D. Ma, W. Song, C. Cao, *J. Am. Chem. Soc.* **2023**, *145*, 12023–12032.
[96] a) J. Wu, L. Xiong, B. Zhao, M. Liu, L. Huang, *Small Methods* **2020**, *4*, 1900540; b) H. Jin, K. Zhou, R. Zhang, H. Cui, Y. Yu, P. Cui, W. Song, C. Cao, *Nat. Commun.* **2023**, *14*, 2494.

[97] a) L. Zhang, K. Doyle-Davis, X. Sun, *in Supported Metal Single Atom Catalysis* (eds P. Serp and D.P. Minh) **2022**, pp. 169–198; b) M. Kottwitz, Y. Li, H. Wang, A. I. Frenkel, R. G. Nuzzo, *Chemistry-Methods* **2021**, *1*, 278–294; c) X. Li, X. Yang, J. Zhang, Y. Huang, B. Liu, *ACS Catal.* **2019**, *9*, 2521–2531; d) A. Casu, S. Ould-Chikh, G. Mountjoy, A. Corrias, A. Falqui, *in Supported Metal Single Atom Catalysis* (eds P. Serp and D.P. Minh) **2022**, pp. 199–239; e) B. B. Sarma, F. Maurer, D. E. Doronkin, J.-D. Grunwaldt, *Chem. Rev.* **2023**, *123*, 379–444.
[98] B. B. Sarma, J. Jelic, D. Neukum, D. E. Doronkin, X. Huang, F. Studt, J.-D. Grunwaldt, *J. Phys. Chem. C* **2023**, *127*, 3032–3046.
[99] Y. Chen, R. Rana, T. Sours, F. D. Vila, S. Cao, T. Blum, J. Hong, A. S. Hoffman, C.-Y. Fang, Z. Huang, C. Shang, C. Wang, J. Zeng, M. Chi, C. X. Kronawitter, S. R. Bare, B. C. Gates, A. R. Kulkarni, *J. Am. Chem. Soc.* **2021**, *143*, 20144–20156.
[100] a) K. Feng, H. Zhang, J. Gao, J. Xu, Y. Dong, Z. Kang, J. Zhong, *Appl. Phys. Lett.* **2020**, *116*, 191903; b) J. Finzel, K. M. Sanroman Gutierrez, A. S. Hoffman, J. Resasco, P. Christopher, S. R. Bare, *ACS Catal.* **2023**, *13*, 6462–6473; c) L. Liu, A. Corma, *Nature Catal.* **2021**, *4*, 453–456.
[101] Y. Zhang, D. T. Tran, D. Baker, S. Zhang, T. Wang, S. Hwang, E. Schulman, J. Fu, W. Zheng, D. G. Vlachos, J. Qi, P. Christopher, Y. Liu, A. Frenkel, D. Liu, *Mol. Catal.* **2022**, *531*, 112709.
[102] C. Copéret, W.-C. Liao, C. P. Gordon, T.-C. Ong, *J. Am. Chem. Soc.* **2017**, *139*, 10588–10596.
[103] Y. Zeng, X. Li, J. Wang, M. T. Sougrati, Y. Huang, T. Zhang, B. Liu, *Chem Catal.* **2021**, *1*, 1215–1233.
[104] a) C. Rivera-Cárcamo, F. Leng, I. C. Gerber, I. del Rosal, R. Poteau, V. Collière, P. Lecante, D. Nechiyil, W. Bacsa, A. Corrias, M. R. Axet, P. Serp, *Catal. Sci. Technol.* **2020**, *10*, 4673–4683; b) Y. Lu, C.-T. Kuo, L. Kovarik, A. S. Hoffman, A. Boubnov, D. M. Driscoll, J. R. Morris, S. R. Bare, A. M. Karim, *J. Catal.* **2019**, *378*, 121–130.
[105] J. Navarro-Ruiz, R. Poteau, I. C. Gerber, I. del Rosal, *in Supported Metal Single Atom Catalysis* (eds P. Serp and D.P. Minh) **2022**, pp. 241–337.
[106] S. Mitchell, F. Parés, D. Faust Akl, S. M. Collins, D. M. Kepaptsoglou, Q. M. Ramasse, D. Garcia-Gasulla, J. Pérez-Ramírez, N. López, *J. Am. Chem. Soc.* **2022**, *144*, 8018–8029.

Manuscript received: April 17, 2023
Revised manuscript received: June 12, 2023
Accepted manuscript online: June 12, 2023
Version of record online: ■■, ■■

REVIEW

Cooperative catalysis: Exploiting the synergy that can exist between single atoms and nanoparticles is a stimulating approach to improve catalytic performance, which opens up perspectives and challenges in terms of catalyst synthesis and characterization. In this mini-review we discuss the main synergies observed to date and discuss selected examples where the origin of the synergy was evidence to elucidate reaction mechanisms.

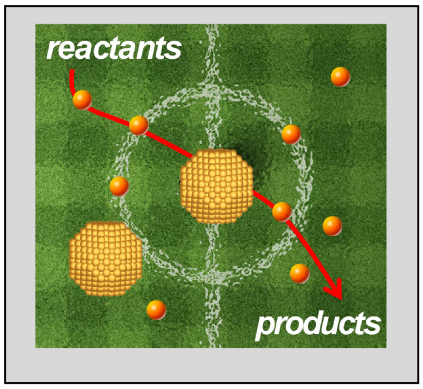

*Prof. Dr. P. Serp**